Research Article | Vol. 24, No. 22 | 31 Oct 2016 | OPTICS EXPRESS 24989

Optics EXPRESS

High-energy two-cycle pulses at 3.2 μm by a broadband-pumped dual-chirped optical parametric amplification

YANCHUN YIN, JIE LI, XIAOMING REN, YANG WANG, ANDREW CHEW, AND ZENGHU CHANG*

Institute for the Frontier of Attosecond Science and Technology, CREOL and Department of Physics, University of Central Florida, Orlando, Florida 32816, USA
*Zenghu.Chang@ucf.edu

Abstract: A design for efficient generation of mid-infrared pulses at 3.2 μm is presented, which is based on numerical simulations of the broadband-pumped dual-chirped optical parametric amplification (DC-OPA) in $LiNbO_3$ doped with 5 mol.% MgO (MgO:$LiNbO_3$). The broadband seed can be generated by difference frequency generation in KTA using spectrally-broadened Ti:Sapphire lasers. The broad DC-OPA phase-matching bandwidth-spanning from 2.4 μm to 4.0 μm-is achieved by chirping both the broadband Ti:Sapphire pump pulses and the seed pulses in such a way that the individual temporal slice of pump spectrum is able to phase match that of seed spectrum. This phase matching scheme allows the use of longer crystals without gain narrowing or loss of conversion efficiency. The theoretical conversion efficiency from the pump to the idler reaches 19.1 %, enabling generation of a few hundred mJ of mid-IR energy with an available large-aperture MgO:$LiNbO_3$ crystal. Furthermore, the commercially available acousto-optic programmable dispersive filter (AOPDF) ensures compression of such a broad bandwidth down to 20 fs (two optical cycles at 3.2 μm).

OCIS codes: (320.7090) Ultrafast lasers; (190.4970) Parametric oscillators and amplifiers.

References and links

1. F. Krausz and M. Ivanov, "Attosecond physics," Rev. Mod. Phys. **81**, 163–234 (2009).
2. Z. Chang, P. B. Corkum, and S. R. Leone, "Attosecond optics and technology: Progress to-date and future prospects (Invited)," J. Opt. Soc. Am. B **33**, 1081–1097 (2016).
3. K. Zhao, Q. Zhang, M. Chini, Y. Wu, X. Wang, and Z. Chang, "Tailoring a 67 attosecond pulse through advantageous phase-mismatch," Opt. Lett. **37**, 3891–3893 (2012).
4. B. Shan and Z. Chang, "Dramatic extension of the high-order harmonic cutoff by using a long-wavelength driving field," Phys. Rev. A **65**, 011804 (2001).
5. E. J. Takahashi, T. Kanai, K. L. Ishikawa, Y. Nabekawa, and K. Midorikawa, "Coherent Water Window X Ray by Phase-Matched High-Order Harmonic Generation in Neutral Media," Phys. Rev. Lett. **101**, 253901 (2008).
6. S. Gilbertson, H. Mashiko, C. Li, E. Moon, and Z. Chang, "Effects of laser pulse duration on extreme ultraviolet spectra from double optical gating," Appl. Phys. Lett. **93**, 111105 (2008).
7. M. Chini, K. Zhao and Z. Chang, "The Generation, Characterization, and Applications of Broadband Isolated Attosecond Pulses," Nat. Photonics **8**, 178–186 (2014).
8. N. Ishii, K. Kaneshima, K. Kitano, T. Kanai, S. Watanabe, and J. Itatani, "Carrier-envelope phase-dependent high harmonic generation in the water window using few-cycle infrared pulses," Nat. Commun. **5**, 3331 (2014)
9. F. Silva, S. M. Teichmann, S. L. Cousin, M. Hemmer, and J. Biegert, "Spatiotemporal isolation of attosecond soft x-ray pulses in the water window," Nat. Commun. **6**, 7611–7616 (2015).
10. J. Li, X. Ren, Y. Yin, Y. Cheng, E. Cunningham, Y. Wu, and Z. Chang, "Polarization gating of high harmonic generation in the water window," Appl. Phys. Lett. **108**, 231102 (2016).
11. H. Fattahi, H. G. Barros, M. Gorjan, T. Nubbemeyer, B. Alsaif, C. Y. Teisset, M. Schultze, S. Prinz, M. Haefner, M. Ueffing, A. Alismail, L. Vámos, A. Schwarz, O. Pronin, J. Brons, X. T. Geng, G. Arisholm, M. Ciappina, V. S. Yakovlev, D.-E. Kim, A. M. Azzeer, N. Karpowicz, D. Sutter, Z. Major, T. Metzger, and F. Krausz, "Third-generation femtosecond technology," Optica **1**, 45–63 (2014).
12. A. Vaupel, N. Bodnar, B. Webb, L. Shah, and M. Richardson, "Concepts, performance review, and prospects of table-top, few-cycle optical parametric chirped-pulse amplification," Opt. Eng. **53**, 051507 (2013).
13. T. Fuji, N. Ishii, C. Y. Teisset, X. Gu, T. Metzger, A. Baltuska, N. Forget, D. Kaplan, A. Galvanauskas, and F. Krausz, "Parametric amplification of few-cycle carrier-envelope phase-stable pulses at 2.1 μm," Opt. Lett. **31**, 1103–1105 (2006).

#273786 http://dx.doi.org/10.1364/OE.24.024989
Journal © 2016 Received 15 Aug 2016; revised 24 Sep 2016; accepted 6 Oct 2016; published 17 Oct 2016

Optics EXPRESS

14. O. D. Mücke, S. Ališauskas, A. J. Verhoef, A. Pugžlys, A. Baltuška, V. Smilgevičius, J. Pocius, L. Giniūnas, R. Danielius, and N. Forget, "Self-compression of millijoule 1.5 μm pulses," Opt. Lett. **34**, 2498–2500 (2009).
15. Y. Deng, A. Schwarz, H. Fattahi, M. Ueffing, X. Gu, M. Ossiander, T. Metzger, V. Pervak, H. Ishizuki, T. Taira, T. Kobayashi, G. Marcus, F. Krausz, R. Kienberger, and N. Karpowicz, "Carrier-envelope-phase-stable, 1.2 mJ, 1.5 cycle laser pulses at 2.1 μm," Opt. Lett. **37**, 4973–4975 (2012).
16. N. Ishii, K. Kaneshima, K. Kitano, T. Kanai, S. Watanabe, and J. Itatani, "Sub-two-cycle, carrier-envelope phase-stable, intense optical pulses at 1.6 μm from a BiB_3O_6 optical parametric chirped-pulse amplifier," Opt. Lett. **37**, 4182–4184 (2012).
17. K.-H. Hong, C.-J. Lai, J. P. Siqueira, P. Krogen, J. Moses, C.-L. Chang, G. J. Stein, L. E. Zapata, and F. X. Kärtner, "Multi-mj, khz, 2.1 μm optical parametric chirped-pulse amplifier and high-flux soft x-ray high-harmonic generation," Opt. Lett. **39**, 3145–3148 (2014).
18. N. Ishii, K. Kaneshima, T. Kanai, S. Watanabe, and J. Itatani, "Sub-two-cycle millijoule optical pulses at 1600 nm from a BiB_3O_6 optical parametric chirped-pulse amplifier," in "CLEO: 2015," (Optical Society of America, 2015), p. SF1M.3.
19. Y. Yin, J. Li, X. Ren, K. Zhao, Y. Wu, E. Cunningham, and Z. Chang, "High-efficiency optical parametric chirped-pulse amplifier in BiB3O6 for generation of 3mJ, two-cycle, carrier-envelope-phase-stable pulses at 1.7 μm," Opt. Lett. **41**, 1142–1145 (2016).
20. S. Wandel, M. Lin, Y. Yin, G. Xu, and I. Jovanovic, "Parametric generation and characterization of femtosecond mid-infrared pulses in $ZnGeP_2$," Opt. Express **24**, 5287–5299 (2016).
21. P. Malevich, T. Kanai, H. Hoogland, R. Holzwarth, A. Baltuska, and A. Pugzlys, "Broadband mid-infrared pulses from potassium titanyl arsenate/zinc germanium phosphate optical parametric amplifier pumped by Tm, Ho-fiber-seeded Ho:YAG chirped-pulse amplifier," Opt. Lett. **41**, 930–933 (2016).
22. D. Sanchez, M. Hemmer, M. Baudisch, S. Cousin, K. Zawilski, P. Schunemann, O. Chalus, C. Simon-Boisson, and J. Biegert, "7 μm, ultrafast, sub-millijoule-level mid-infrared optical parametric chirped pulse amplifier pumped at 2 μm," Optica **3**, 147–150 (2016).
23. K. Kaneshima, N. Ishii, K. Takeuchi, and J. Itatani, "Generation of carrier-envelope phase-stable mid-infrared pulses via dual-wavelength optical parametric amplification," Opt. Express **24**, 8660–8665 (2016).
24. P. Krogen, H. Liang, K. Zawilski, P. Schunemann, T. Lang, U. Morgner, J. Moses, F. Kaertner, and K. Hong, "Octave-spanning 1.5-optical-cycle 6.5-μm OPA pumped by 2.1-μm OPCPA," in Conference on Lasers and Electro-Optics, OSA Technical Digest (2016) (Optical Society of America, 2016), paper STu3I.4.
25. M. Bock, L. von Grafenstein, U. Griebner, and T. Elsaesser, "Picosecond 40 mJ, 1 kHz Ho:YLF Amplifier at 2 μm," in Conference on Lasers and Electro-Optics, OSA Technical Digest (2016) (Optical Society of America, 2016), paper STu4M.4.
26. C.J. Fecko, J.J. Loparo, A. Tokmakoff, "Generation of 45 femtosecond pulses at 3 μm with a $KNbO_3$ optical parametric amplifier," Opt. Commun. **241**, 521–528 (2004).
27. D. Brida, C. Manzoni, G. Cirmi, M. Marangoni, S. De Silvestri, and G. Cerullo, "Generation of broadband mid-infrared pulses from an optical parametric amplifier," Opt. Express **15**, 15035–15040 (2007).
28. D. Brida, M. Marangoni, C. Manzoni, S. Silvestri, and G. Cerullo, "Two-optical-cycle pulses in the mid-infrared from an optical parametric amplifier," Opt. Lett. **33**, 2901–2903 (2008).
29. O. Chalus, P. Bates, M. Smolarski, and J. Biegert, "Mid-IR short-pulse OPCPA with micro-Joule energy at 100 kHz," Opt. Express **17**, 3587–3594 (2009).
30. C. Erny, C. Heese, M. Haag, L. Gallmann, and U. Keller, "High-repetition-rate optical parametric chirped-pulse amplifier producing 1-μJ, sub-100-fs pulses in the mid-infrared," Opt. Express **17**, 1340–1345 (2009).
31. K. Zhao, H. Zhong, P. Yuan, G. Xie, J. Wang, J. Ma, and L. Qian, "Generation of 120 GW mid-infrared pulses from a widely tunable noncollinear optical parametric amplifier," Opt. Lett. **38**, 2159–2161 (2013).
32. G. Andriukaitis, T. Balciunas, S. Alisauskas, A. Pugzlys, A. Baltuska, T. Popmintchev, M. Chen, M. Murnane, and H. Kapteyn, "90 GW peak power few-cycle mid-infrared pulses from an optical parametric amplifier," Opt. Lett. **36**, 2755–2757 (2011).
33. Q. Zhang, E. Takahashi, O. Mücke, P. Lu, and K. Midorikawa, "Dual-chirped optical parametric amplification for generating few hundred mJ infrared pulses," Opt. Express **19**, 7190–7212 (2011).
34. Y. Fu, E. Takahashi, and K. Midorikawa, "High-energy infrared femtosecond pulses generated by dual-chirped optical parametric amplification," Opt. Lett. **40**, 5082–5085 (2015).
35. Y. Fu, E. Takahashi, Q. Zhang, P. Lu, and K. Midorikawa, "Optimization and characterization of dual-chirped optical parametric amplification," J. Opt. **17**, 124001 (2015).
36. B. E. Schmidt, N. Thire, M. Boivin, A. Laramee, F. Poitras, G. Lebrun, T. Ozaki, H. Ibrahim, and F. Legare, "Frequency domain optical parametric amplification," Nat. Commun. **5**, 3643 (2014)
37. Y. C. Yin, D. French, and I. Jovanovic, "Ultrafast temporal pulse shaping via phase-sensitive three-wave mixing," Opt. Express **18**, 18471–18482 (2010)
38. Y. R. Shen, *The Principles of Nonlinear Optics* (Wiley, 2003).
39. M. D. Feit and J. A. Fleck, Jr., "Computation of mode properties in optical fiber waveguides by a propagating beam method," Appl. Opt. **19**, 1154–1164 (1980).
40. H. Fattahi, A. Schwarz, S. Keiber, and N. Karpowicz, "Efficient, octave-spanning difference-frequency generation using few-cycle pulses in simple collinear geometry," Opt. Lett. **38**, 4216–4219 (2013).

Optics EXPRESS

41. H. Suchowski, P. Krogen, S. Huang, F. Kärtner, and J. Moses, "Octave-spanning coherent mid-IR generation via adiabatic difference frequency conversion," Opt. Express **21**, 28892–28901 (2013).
42. C. Giulio and D. Sandro, "Ultrafast optical parametric amplifiers," Rev. Sci. Instrum. **74**, 1–18 (2003).
43. C. Li, E. Moon, and Z. Chang, "Carrier-envelope phase shift caused by variation of grating separation," Opt. Lett. **31**, 3113–3115 (2006).
44. R.M. Wood, *Laser Damage in Optical Materials* (Hilger, Boston, 1986).

1. Introduction

Attosecond science, one of the fastest advancing frontiers in ultrafast laser research, has opened a new era of understanding electron dynamics and correlations that occur on attosecond timescales [1, 2]. So far, isolated attosecond pulses as short as 67 as have been generated in an extreme ultraviolet (XUV) wavelength range via high harmonic generation (HHG) driven by spectrally-broadened Ti:Sapphire lasers at ~ 800nm [3]. The single atom cutoff photon energy of HHG is $3.2U_p + I_p$, where I_p refers to the atom ionization potential and U_p is the ponderomotive potential that is proportional to the product of the driving laser intensity and wavelength squared. It is evident that both an increase in the driving pulse intensity and its wavelength can lead to cutoff extension. Since the maximum intensity that can be applied for HHG is limited by phase matching and depletion of the neutral gas target, longer wavelength laser sources are needed to extend the cutoff [4, 5]. In addition, because an attosecond pulse is generated every half cycle of the driving laser, few-cycle driving pulses are preferred in order to efficiently generate isolated attosecond pulses with sub-cycle gating [6, 7]. Rapid development of few-cycle and high-energy driving lasers with center wavelengths varying from 1.6 μm to 2.1 μm in recent years has already enabled the generation of the attosecond soft X-ray pulses in water-window region (280 to 530 eV) [8–10]. To significantly increase both center photon energy and bandwidth of attosecond X-ray pulses, the development of high-energy few-cycle pulses further into mid-infrared (mid-IR) region is in demand.

High-energy few-cycle infrared pulses are primarily enabled by optical parametric chirped pulse amplification (OPCPA) pumped by few-picosecond (ps) lasers, which allows a trade-off between the gain bandwidth and the damage threshold of the nonlinear crystals [11, 12]. Among a number of few-cycle IR OPCPA sources that have been reported [13–19], only a few of them yielded mJ-level near-octave pulses (two cycles and below) [15, 18, 19]. Recently, rapid progress has been made on the generation of mid-IR laser sources around 5 μm or above [20–24], among which μJ-level 5-11 μm [23] and 4.5-9 μm [24] laser pulses can be potentially amplified to achieve mJ-level energy by OPCPA in ZGP pumped by a 2.0 μm Ho:YAG laser [25]. The generation of few-cycle pulses or the bandwidth needed for supporting few-cycle pulses near 3 μm by optical parametric amplification (OPA) [26–28] has also been reported. However, upscaling to mJ level in those systems is difficult. OPCPA systems have yielded high energy but long pulses [29–32]. Thus, it has been a challenging task to generate high-energy few-cycle pulses around 3 μm.

In this paper, we present a design for generating high-energy two-cycle pulses at 3.2 μm using broadband-pumped dual-chirped optical parametric amplification (DC-OPA) in $LiNbO_3$ doped with 5 mol.% MgO (MgO:$LiNbO_3$). DC-OPA [33] is essentially an OPCPA pumped by chirped pulses. While DC-OPA has been both numerically analyzed [33] and experimentally utilized and analyzed [34, 35], it has not been studied from the perspective of phase matching between the individual temporal slice of pump spectrum and that of seed spectrum, an approach that is more intuitive. By analyzing the phase matching in a MgO:$LiNbO_3$ DC-OPA, we have found that a broadband Ti:Sapphire pump and a broadband seed (2.3-4.1 μm) can phase match very well in the temporal domain if their chirps are managed properly. Unlike the common few-cycle OPCPA and DC-OPA, this broadband-pumped DC-OPA allows the use of longer crystals without either gain narrowing or efficiency loss since phase matching occurs between the individual temporal slice of pump spectrum and that of seed spectrum. A method is presented for the

Optics EXPRESS

generation of carrier-envelope phase (CEP)-stable broadband seed pulses via difference frequency generation (DFG) in KTA, allowing the separation of the idler beam from the signal beam and amplification of the idler beam without introducing angular spatial chirp in the DC-OPA. Furthermore, the choice of chirping material and the pulse compression method are provided. This broadband-pumped DC-OPA has a great advantage over the narrowband-pumped OPCPA with respect to the phase matching bandwidth, especially in the nondegenerate configuration where the phase matching bandwidth is usually narrow; it also has advantages over frequency domain optical parametric amplification (FOPA) [36] in that it can preserve the CEP of the seed pulse and compress the pulse in a bulk material almost without loss of pulse energy, while FOPA tends to deteriorate the CEP of the seed pulse if without an active feedback, as well as results in loss of pulse energy because of compression using gratings.

2. Numerical model for three-wave mixing

To simulate DFG and DC-OPA, a one-dimensional three-wave mixing numerical model has been developed by modifying the previously developed one in [37]: (1) the model includes the effects of dispersion and nonlinear refractive index due to self phase modulation (SPM) and cross phase modulation (XPM); (2) all three waves are assumed to be plane waves. The model uses standard coupled differential equations with the slowly varying envelope approximation for three-wave mixing [38]:

$$\frac{dA_1}{dz} = j\frac{2d_{eff}\omega_1^2}{k_1c^2}A_2^*A_3\exp(-j\Delta kz), \tag{1}$$

$$\frac{dA_2}{dz} = j\frac{2d_{eff}\omega_1^2}{k_2c^2}A_1^*A_3\exp(-j\Delta kz) \tag{2}$$

$$\frac{dA_3}{dz} = j\frac{2d_{eff}\omega_3^2}{k_3c^2}A_1A_2\exp(j\Delta kz), \tag{3}$$

where $A_{1,2,3}$ are the complex field amplitudes of the signal, idler, and pump waves, respectively, d_{eff} is the second-order effective nonlinearity, ω_i is the angular frequency, k_i is the wave vector, Δk is the wave vector mismatch, and c is the speed of light in vacuum. The longitudinal coordinate is denoted by z. To address the important temporal characteristics of this process, the complex amplitude of the signal and pump pulses A_i are represented in the time and frequency domain: A_i=$A_i(t)$=$F^{-1}[A_i(\omega)]$, including the corresponding amplitude and phase. While the coupled differential equations for the three fields are expressed and integrated in the time domain, it is also necessary to include dispersion, which is easily represented in the spectral domain. Dispersion is included in the model using the usual split-step approach [39], by transforming the fields into the spectral domain after each step of numerical integration in the time domain. The spectral phase applied to the three fields at each step is

$$A_i(\omega) \rightarrow A_i\,(\omega)\exp(jn_i(\omega)\omega\,dz/c)\,, \tag{4}$$

where ω is the angular frequency, and $n(\omega)$ is the refractive index for the corresponding spectral component ω of wave A_i. Self phase modulation and cross phase modulation are included in the model by applying the temporally-dependent phase to each wave

$$A_i(t) \rightarrow A_i(t)\exp(jn_2^{SPM}\omega_i I_i(t)\,dz/c), \tag{5}$$

$$A_{1,2}(t) \rightarrow A_3(t)\exp(jn_2^{XPM}\omega_i I_i(t)\,dz/c), \tag{6}$$

where n_2^{SPM} and n_2^{XPM} are the nonlinear refractive indexes of SPM and XPM, respectively, $I_i(t)$ is the instantaneous intensity at time t, and ω_i is the center frequency of wave A_i. The XPM

Optics EXPRESS

effects on the pump pulse can be neglected because of the low intensities of the signal and idler pulses. The traveling frame of reference for the calculation is established in reference to the signal wave A_1 by applying the linear phase after each split step:

$$A_i(\omega) \rightarrow A_i\ (\omega) \exp(jn_1(\omega_1)\omega_1\ dz/c)\,, \tag{7}$$

where $n_1(\omega_1)$ is the refractive index for the signal wave at the signal center frequency ω_1.

3. Broadband seed generation via DFG in KTA

Difference frequency generation is a common approach to producing broadband seed pulses with passive carrier-envelope phase stabilization [23, 24, 40, 41]. Here we propose and numerically simulate the generation of broadband seed from DFG in a KTA crystal. The KTA crystal is cut at 41.5° in the XZ plane. The spectra of the pump (700 nm) and signal (913 nm) are both super Gaussian and have a FWHM bandwidth of 50 nm. Both the input pump and signal intensities are 200 GW/cm^2. Different thicknesses of KTA crystals are considered in order to find a compromise between bandwidth and conversion efficiency. Fig. 1 shows DFG spectra for three examples of KTA thickness. The 0.1 mm KTA produces a broadest bandwidth-spanning from around 2.3 μm to 4.5 μm and has a conversion efficiency of 1.1 %, while the 0.15mm and 0.2 mm KTAs produce narrower bandwidth but higher conversion efficiency-1.8 % and 2.4 %, respectively. Since seed bandwidth is the primary concern, 0.1 mm KTA is chosen for seeding DC-OPA. The proof-of-principle experiment for demonstrating this DFG process can be done with mJ level broadened Ti:Sapphire spectrum in a hollow-core fiber (HCF) that typically ranges from 0.55 μm to 0.95 μm. This approach could generate a μJ-level CEP-stable broadband pulse for seeding the broadband-pumped DC-OPA discussed in this paper.

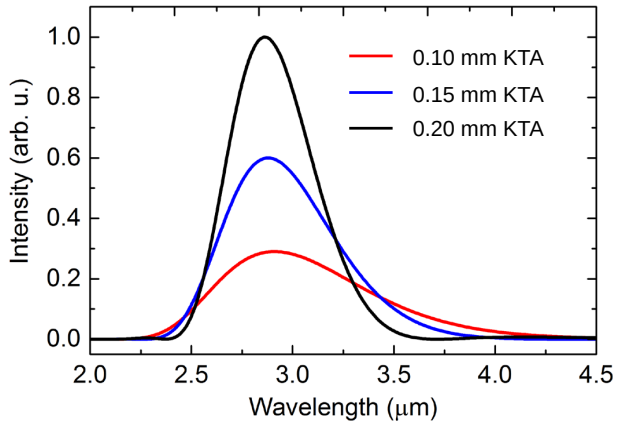

Fig. 1. DFG spectra in KTA crystals with different thicknesses, cut at 41.5° in the XZ plane.

4. Achieving broad gain bandwidth in DC-OPA

The phase matching bandwidth in OPA is given to the first order by $\Delta\omega \sim 1/\mathrm{v}_{gs}$-$1/v_{gi}$, where v_{gs} and v_{gi} are the group velocities of the signal and idler, respectively. Thus, broadband parametric gain can be achieved when the group velocities of signal and idler are matched [42]. As expected, broadband parametric gain occurs in the degenerate configuration, where signal and idler have the same wavelength and polarization. For the generation of broadband 3 μm sources, the group-velocity matching condition in a nondegenerate OPA configuration has been demonstrated, where the group velocity of signal wavelength around 1 μm is close to that of the

Optics EXPRESS

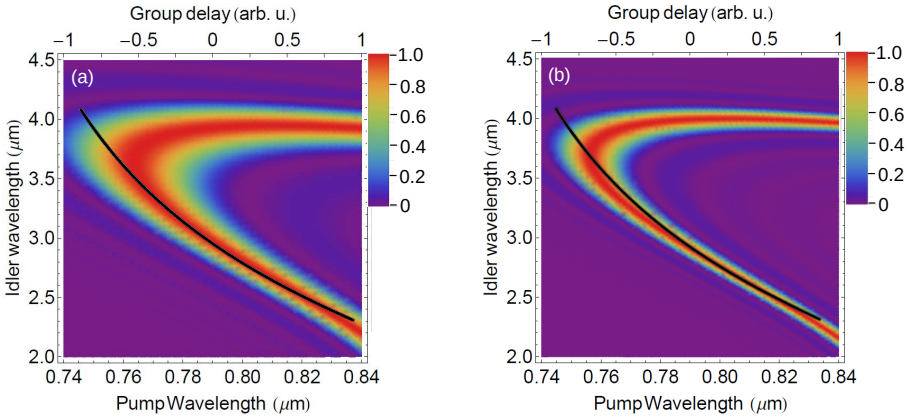

Fig. 2. The calculated phase-matching efficiency as a function of pump and idler wavelengths for a noncollinear configuration (PM angle θ = 44.4°, noncollinear angle α = 0.5°). The black line represents the chirped signal pulse with its corresponding wavelengths marked by the left axis and its temporal chirp marked by the top axis. (a) 2 mm MgO:$LiNbO_3$; (b) 4 mm MgO:$LiNbO_3$.

idler wavelength around 3 μm when pumped by a 800 nm Ti:Sapphire laser [26–28]. However, the bandwidth generated in those OPAs is still not enough to support two-cycle or shorter pulses near 3 μm. Moreover, the OPCPA, which is needed to generate high-energy laser pulses, suffered from loss of gain bandwidth [29–32].

By searching and studying the phase matching of nonlinear crystals, we have found that MgO:$LiNbO_3$ has a broad gain bandwidth around 3 μm when pumped by a broadband (0.74 nm - 0.84 nm) Ti:Sapphire laser, as shown in Fig. 2. Moreover, the phase matching condition can be met in the temporal domain in the broadband-pumped DC-OPA when the chirps of the pump pulse and the idler pulse are matched. Actually, the most critical aspect for realizing such a broad parametric gain bandwidth in the DC-OPA is the dispersion management. With the pump pulse being almost linearly stretched by using conventional grating pairs, the scheme of stretching the idler pulse is important for phase matching. For stretching the idler pulses, gratings pairs are not considered because of the CEP variation that requires active stabilization [43]. Here an acousto-optic programmable dispersive filter (AOPDF) stretcher plus a bulk material compressor are employed to take advantage of the adaptive phase control capability of the AOPDF and the high throughput and compactness of the bulk material. Since the pulse-lengthening pre-chirp of the AOPDF stretcher must be chosen to match the inflexible pulse-shortening de-chirp of the bulk material, the choice of bulk materials is very important. Third-order dispersion (TOD) and other higher order dispersions would contribute to a nonlinear chirp, leading to poor phase matching between the idler and the pump in the temporal domain. Thus, in order to stretch the idler pulse almost linearly with AOPDF, the corresponding ideal bulk material should have a high ratio between the second-order dispersion (GDD) and higher-order dispersions, especially TOD. Table 1 shows dispersion properties of four typical infrared materials. Si is chosen for chirping idler pulses because of its moderate bandgap, relatively large GDD, and a largest ratio between GDD and TOD.

In Fig. 2, the phase matching efficiency, $\mathrm{sinc}^2(\Delta kL/2)$, is plotted as a function of the pump (bottom axis) and idler wavelengths (left axis), where Δk represents phase mismatch and L is the MgO:$LiNbO_3$ crystal length. The color contours represent the phase matching efficiency. The black line demonstrates both the spectrum (left axis) and the group delay (top axis) of the idler pulse chirped by the AOPDF. The pump spectrum is assumed to be linearly stretched and its

Optics EXPRESS

Table 1. Dispersion of bulk material at 3 μm.

Materials (10 mm)	GDD (fs^2)	TOD (fs^3)	FOD (fs^4)
Si	4087	1695	−29667
Ge	15248	31689	39984
ZnS	608	4564	−17271
ZnSe	1609	4401	−7642

temporal information is also shown by top axis. Fig. 2 can completely reveal the phase matching between the idler and the pump in both the temporal domain and spectral domain. For a 2 mm crystal thickness, the black curve (Fig. 2(a)) can fit in the best phase matching region very well, indicating excellent phase matching between the idler and pump over a broad bandwidth spanning from 2.3 μm to 4.0 μm. When the crystal thickness is doubled to 4 mm, the black curve (Fig. 2(b)) is still within the best phase matching region. Therefore, it is expected that the broadband-pumped DC-OPA, which employs the design of phase matching in $MgO:LiNbO_3$, allows the use of a longer crystal without sacrificing either parametric gain or bandwidth, unlike typical few-cycle narrowband-pumped OPCPA.

5. Simulation of DC-OPA

To further study the broad parametric gain bandwidth in the DC-OPA, two simulations were performed for two different crystal length under different pump conditions. To characterize and compare parametric interactions for different crystal length, it is necessary to calculate the parametric gain, which is defined as [42]:

$$G = \frac{I_s(L_c)}{I_{s0}} = \frac{1}{4}\exp(2\Gamma L_c), \tag{8}$$

which grows exponentially with the crystal length L_c and nonlinear coefficient Γ, given as

$$\Gamma^2 = \frac{8\pi^2 d_{\text{eff}}^2 I_p}{n_i n_s n_p \lambda_i \lambda_s \epsilon_0 c_0}, \tag{9}$$

where d_{eff} is the effective nonlinearity, I_p is the pump intensity, $n_{i,s,p}$ are the refractive indices of the idler, signal, and pump wavelengths respectively, $\lambda_{i,s}$ are the wavelengths of the idler and signal, respectively, ϵ_0 is the vacuum permittivity, and c_0 is the speed of light in vacuum. Thus, the parametric gain grows exponentially with the crystal length and square root of intensities.

In both simulations, the input idler spectrum spanning from 2.4 μm to 4.0 μm is from the DFG spectrum produced in a 0.1 mm KTA crystal. The pump spectrum spanning from 740 nm to 840 nm has a super Gaussian shape. $MgO:LiNbO_3$ is chosen as the DC-OPA crystal, which has a type I configuration with a phase matching angle of 44.4 °. A small nonlinear angle of 0.5 ° is introduced in order to separate the idler from the signal.

In the first simulation, the signal is negatively stretched to 1.0 ps (2.4 μm to 4.0 μm) by the AOPDF with a chirp value equal to the opposite chirp induced by an 8 mm silicon. The pump is positively linearly stretched to 1.79 ps (740 nm to 840 nm). The input idler and pump intensities are 12 MW/cm^2 and 30 GW/cm^2, respectively. $MgO:LiNbO_3$ has a high damage threshold and can withstand 50 GW/cm^2 intensity from a 1.6 ps Yb:YAG thin disk laser [15]. Here we assume that 30GW/cm^2 intensity from a chirped 1.79 ps Ti:Sapphire laser is below the damage threshold of $MgO:LiNbO_3$. The optimized crystal thickness is 2.4 mm in order to obtain a maximum conversion efficiency. The simulation results are shown in Fig 3. As shown in Fig 3(a), an initial delay of 150 fs between the idler and the pump is introduced in order to compensate for the temporal walkoff that can deteriorate the phase matching condition. As can be seen from Fig 3(c),

Optics EXPRESS

the amplified idler spectrum spans from 2.4 μm to 4.0 μm, supporting a 20.4 fs transform-limited pulse-two-cycle pulse at 3.2 μm-shown in Fig 3(d). Moreover, the pump to idler conversion efficiency reaches 19.1 %, resulting from the almost depleted pump over a broad bandwidth shown in Fig 3(d). The idler gain of 954 is typical, amplifying a nJ level pulse to μJ level.

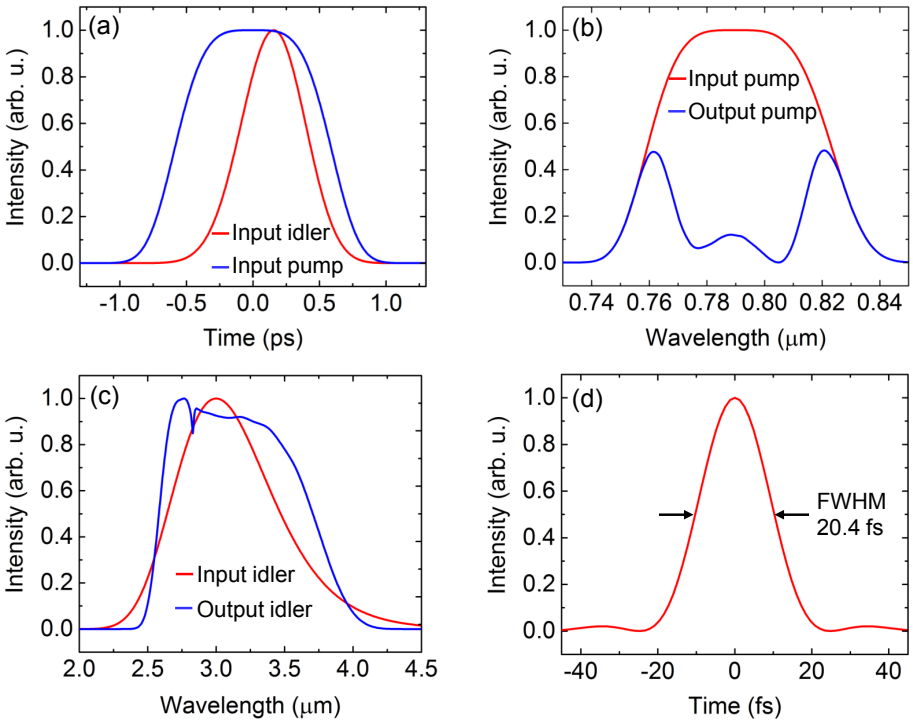

Fig. 3. Simulation results of the broadband-pumped DC-OPA in a 2.4 mm MgO:$LiNbO_3$.

The energy scaling capability of common few-cycle OPCPA and DC-OPA is limited not only by the available crystal aperture size, but also by the crystal length when gain bandwidth has to be preserved. While the energy scaling capability of the two-cycle DC-OPA discussed here is also limited by the available crystal size, it is not limited by the crystal length. The second simulation aims to study the energy scaling capability of the DC-OPA with a doubled crystal length, assuming that the aperture size and thus the beam size in the two simulations are same. To get a gain similar to that in the first simulation, the second simulation used 7.5 GW/cm^2 pump intensity, a quarter of the 30 GW/cm^2 used in the first simulation, since the parametric gain grows exponentially with the crystal length and the square root of intensity, as shown in Equation (8) & (9). Here we assume that the damage fluence scales with the root square of pulse duration [44].

In the second simulation, the signal is stretched to 16 ps, which is close to the maximum chirping capability of the AOPDF in the idler spectral region, while the pump pulse duration is optimized to 22.7 ps. Thus, the fluence of the pump in the second simulation is 3.17 times that in the first simulation. This fluence is safe for the crystal according to fluence scaling law with pulse duration, which indicates that 3.56 times the pump fluence in the first simulation can be safely used in the second simulation.The input idler is set to 2.4 MW/cm^2 in order to maintain the same ratio of the input idler energy to the pump energy as used in the first simulation. An initial delay of 200 fs between the idler and the pump is introduced. The simulation results for 4.8 mm crystal are shown in Fig. 4. As expected from the discussion in section 4, there is almost no loss of parametric gain or bandwidth. The amplified spectrum is still similar, supporting a 20.8 fs

Optics EXPRESS

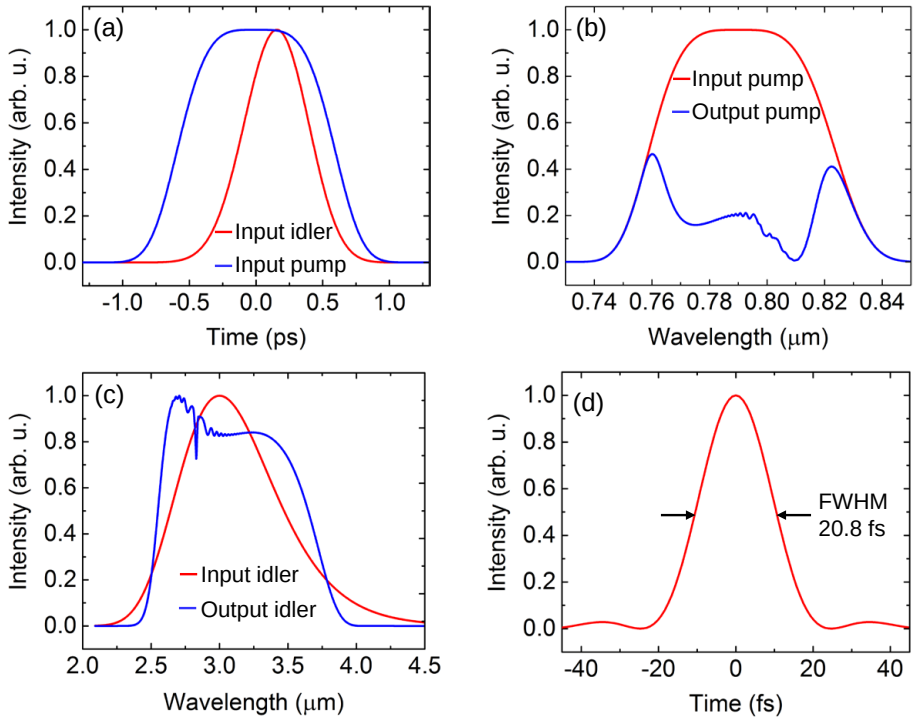

Fig. 4. Simulation results of the broadband-pumped DC-OPA in a 4.8 mm MgO:$LiNbO_3$.

transform-limited pulse. The pump to idler conversion efficiency reaches 18.7%. This further confirms that the design of DC-OPA allows for the use of longer crystals without sacrificing either gain bandwidth or efficiency. For the two simulations discussed here, about 3 times the idler energy can be achieved by using 2 times the crystal thickness. Considering its high second-order nonlinearity (4.2 V/pm) and commercially available large size (20 mm), MgO:$LiNbO_3$ is able to generate high-energy two-cycle pulses at 3.2 μm via DC-OPA.

The optimum pulse duration ratio between the pump and the idler for best phase matching is dependent on the MgO:$LiNbO_3$ crystal length because of the temporal walkoff (~ 0.1 ps/mm) between the pump and the idler in the crystal. In a fixed chirp design, the ratio increases when the crystal is longer in order to compensate for the increased temporal walkoff. In addition, the optimum ratio is more sensitive to the change of crystal length in a relatively small chirp design such as 1 ps design in the first simulation, but is much less sensitive in a relatively large chirp design such as the 16 ps design in the second simulation.

6. Design for a proof-of-principle experiment to demonstrate two-cycle pulses at 3.2 μm via DC-OPA

Here we propose a scheme to demonstrate two-cycle pulses at 3.2 μm via the DC-OPA pumped by a 30 mJ femtosecond Ti:Sapphire laser at 1 kHz. The layout is shown in Fig. 5. Nanojoule-level oscillator pulses is boosted to 30 mJ (740 nm to 840 nm) in a CPA laser system. The output is split into two beams. First, 28 mJ, compressed to around 1.79 ps, is used to pump a three-stage DC-OPA. The remaining 2.0 mJ portion, compressed to 20 fs, is sent to a hollow-core fiber (HCF) filled with neon for white light generation. The white light can be compressed to <7 fs using chirped mirrors. A broadband IR (2.3-4.5 μm) seed is proposed to be generated via DFG from the white light in a 0.1 mm type-II KTA crystal (phase matching angle θ = 41.5°). The seed is then

Optics EXPRESS

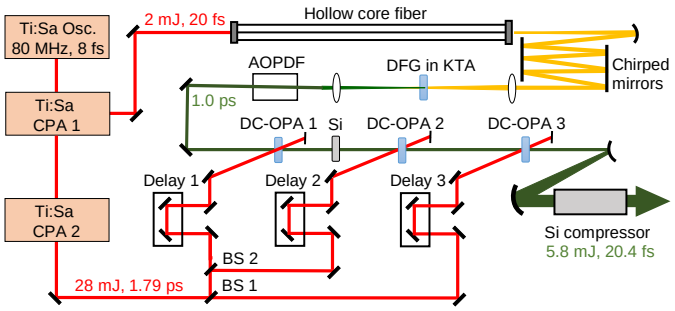

Fig. 5. Schematic drawing for a proof-of-principle experiment for demonstrating DC-OPA.

stretched to 1.0 ps (2.4-4.0 μm) using an AOPDF that has about 10 % throughput over such a broadband. The idler pulse can be amplified in a three-stage DC-OPA in MgO:$LiNbO_3$. The pump energies for the three stages are 0.5 mJ, 4.5 mJ, and 23 mJ, respectively, and the corresponding conversion efficiencies are 19.2%, 18.5%, and 21.4%, respectively. Because the signal pulse is chirped more than the pump pulse in the first-stage 2.4 mm MgO:LiNbO3 crystal, a 4 mm silicon plate is inserted after the first stage in order to reoptimize the pulse duration ratio between the signal and the pump pulses for both the second stage and the third stage. The amplified pulses are compressed by silicon to near transform limit (20.4 fs-two cycles at 3.2 μm) when the high order phase errors are corrected by the AOPDF. In order to achieve ~19% conversion efficiency in the simulation in which a square pulse shape and a square spatial beam are assumed, the ideal spectrum (740 nm to 840 nm) and spatial beam should have a flat-top shape, which can be done without much difficulty. Thus, a 5.8 mJ, two-cycle pulse at 3.2 μm is expected with 28 mJ Ti:Sapphire pump energy and ~19% conversion efficiency. Moreover, hundreds of mJ such pulses can be generated with a joule-level broadband 10 Hz Ti:Sapphire pump and can be compressed with high-bandgap materials such as ZnS.

7. Conclusions

In summary, we provide, for the first time to the best of our knowledge, an approach for efficient generation of mJ-level two-cycle pulses at 3.2 μm based on the results of numerical simulations of the broadband-pumped DC-OPA in MgO:$LiNbO_3$. The broad parametric gain bandwidth, 2.4 μm to 4.0 μm, is achieved by phase matching the individual slice of idler spectrum with the individual slice of pump spectrum in the temporal domain. Unlike the phase matching of common few-cycle OPCPA and DC-OPA, this technique of phase matching allows using longer crystals without losing either gain bandwidth or conversion efficiency. The theoretical conversion efficiency, 19.1%, enables generation of hundreds of mJ two-cycle pulses at 3.2 μm in the DC-OPA with a 20-mm-diameter MgO:$LiNbO_3$ crystal as the parametric gain medium. Further experimental demonstration of such a laser system will pave the way to the generation of a bright broadband soft X-ray continuum, thus enabling attosecond pulses shorter than the atomic unit of time (24 as).

Funding

This work has been supported Army Research Office (W911NF-14-1-0383, W911NF-15-1-0336); Air Force Office of Scientific Research (FA9550-15-1-0037); the DARPA PULSE program by a grant from AMRDEC (W31P4Q1310017). This material is also based upon work supported by the National Science Foundation under Grant Number (NSF Grant Number 1506345). Any opinions, findings, and conclusions or recommendations expressed in this material are those of the authors and do not necessarily reflect the views of the National Science Foundation.